

29

30 ■ INTRODUCTION

31 Secondary organic aerosol (SOA) refers to the aerosol material that is mainly formed by the
 32 atmospheric gas-phase oxidation of volatile organic compounds (VOCs) (Kroll and Seinfeld,
 33 2008; Ziemann and Atkinson, 2012; Seinfeld and Pandis, 2016). Atmospheric oxidation of
 34 VOCs increases the oxygen to carbon ratios (O:C) in the oxidation products and can form
 35 highly oxygenated organic molecules (HOMs). These low volatility products are found to play
 36 a key role in the formation and growth of SOA (Ehn et al., 2014; Öström et al., 2017; Bianchi
 37 et al., 2019; Brean et al., 2019, 2020). However, heterogeneous and multiphase chemistry
 38 involving the reactions of organic compounds directly onto solid particles or inside liquid
 39 particles can also be an important contributor to SOA mass (Ervens et al., 2011, 2014; Kuang
 40 et al., 2020; Gu et al., 2023). The SOA is a dominant component of tropospheric fine particulate
 41 matter (Hallquist et al., 2009; Spracklen et al., 2011; Huang et al., 2014), influences oxidative
 42 capacity, local and global air quality, climate change, and human health (Jacobson et al., 2000;
 43 Hansen and Sato, 2001; Kanakidou et al., 2005; Zhang et al., 2014). Despite having significant
 44 attention due to its importance on SOA, its sources and formation processes are yet to be fully
 45 understood.

46 Aldehydes are common emissions in natural and polluted environments and have both
 47 biogenic and anthropogenic sources (Lipari et al., 1984; Carlier et al., 1986; Ciccioli et al.,
 48 1993; Schauer et al., 1999a, 1999b, 2001) and are also formed by chemical transformation of
 49 other VOCs, especially ozonolysis of alkenes (Calogirou et al., 1999). Atmospheric
 50 degradation of aldehydes is mainly governed by photolysis and the reaction with OH radicals
 51 in the daytime (Mellouki et al., 2003; Calvert et al., 2011; Mellouki et al., 2015). During
 52 nighttime, the reactions with NO_3 radicals are the dominant sink of aldehydes (Calvert et al.,
 53 2011). Although there are prior kinetic studies of reactions of n -aldehydes with OH radicals
 54 available in the literature (Albaladejo et al., 2002; Cassanelli et al., 2005; Iuga et al., 2010;

55 Castañeda et al., 2012; Wang et al., 2015; Aguirre et al., 2025), they are limited to the initial
56 steps of oxidation except recent studies (Barua et al., 2023; Yang et al., 2024) showing further
57 oxidation steps leading to the formation of more functionalized products including HOMs.

58 It is well understood that the reaction of aldehydes with OH radicals is predominantly
59 initiated by the abstraction of aldehydic hydrogen atom due to its weaker bond strength.
60 However, with the increase of carbon chain length, the abstraction of other hydrogen atoms
61 distant from the aldehydic moiety can also contribute to the overall oxidation process. The
62 aldehydic H abstraction can lead to the cleavage of that carbon (C1) by CO loss from acyl
63 (RC(O)) intermediate (Rissanen et al., 2014; Barua et al., 2023). Alternatively, it leads to the
64 acyl peroxy (RC(O)OO) and, in high NO_x (NO + NO₂) condition, subsequently to acyloxy
65 (RC(O)O) intermediate followed by CO₂ loss ultimately forming C_{n-1} aldehyde, C_{n-1} alkyl
66 nitrate, and C_{n-1} alkoxy isomerization products (Vereecken & Peeters, 2009; Chacon-Madrid
67 et al., 2010). Besides, it can also produce C_n peroxyacyl nitrates (PAN) via RC(O)OO + NO₂
68 reaction (Mellouki et al., 2003; Chacon-Madrid et al., 2010; Calvert et al., 2011; Mellouki et
69 al., 2015), a reservoir species for long-range transport of NO_x in the free troposphere.
70 Additionally, C_n peroxy acids can be formed by the reaction of RC(O)OO intermediate and
71 HO₂ (Barua et al., 2023).

72 Chacon-Madrid et al. (2010) have conducted a comparative study of the SOA yields in
73 OH-initiated oxidation of *n*-aldehydes and *n*-alkanes under high NO_x conditions. They reported
74 near identical SOA yields from *n*-tridecanal and *n*-dodecane where the precursor alkane is
75 having one less carbon than the precursor aldehyde. The finding was attributed to the formation
76 of C₁₂ alkoxy radical intermediate from both precursors undergoing similar subsequent
77 reactions leading to SOA. This indicates that the dominant fate of aldehyde oxidation by OH
78 leads to the fragmentation of its carbon backbone losing one carbon atom rather than producing
79 functionalized products with the same number of carbon atoms as the parent molecule.

80 In low NO_x conditions, previous experimental studies have shown that the abstraction
81 of the aldehydic hydrogen can also lead to molecular functionalization forming HOMs (Ehn et
82 al., 2014; Rissanen et al., 2014; Tröstl et al., 2016; Wang et al., 2021) and potentially promote
83 the SOA yields. Recently, Barua et al. (2023) have studied hexanal OH oxidation reaction in
84 detail using high level quantum chemical computations as well as experimental mass
85 spectrometry technique. They showed that both the aldehydic and non-aldehydic H abstraction
86 pathways can contribute to the functionalization of hexanal resulting in rapid formation of
87 HOMs via autoxidation. Autoxidation refers to chain radical processes, generally starting with
88 an oxygen-centered radical that undergoes unimolecular isomerization reaction leading to a

89 carbon-centered radical species whose dominant fate is to add additional molecular oxygen and
90 thus increases product O:C ratios (Crouse et al., 2013; Jokinen et al., 2014; Rissanen et al.,
91 2014; Berndt et al., 2015; Mentel et al., 2015; Rissanen et al., 2015; Berndt et al., 2016). Along
92 the aldehydic H abstraction reaction route, the fastest isomerization (1,6 H-shift rate
93 coefficient, $k = 0.2 \text{ s}^{-1}$) of the RC(O)OO intermediate was shown to be the key for autoxidation
94 reaction chain propagation and competitive with any bimolecular reaction mediated RC(O)O
95 fragmentation (Barua et al., 2023). Thus, the RC(O)OO isomerization reaction (Seal et al.,
96 2023) keeps the carbon backbone of the precursor aldehyde intact. A non-aldehydic H
97 abstraction from C4 was also seen to be competitive and its corresponding RO₂ was shown to
98 undergo a 1,6 H-shift reaction with the aldehydic H atom at a higher rate ($k = 0.9 \text{ s}^{-1}$) than the
99 H-shifts in RC(O)OO radical. The fast aldehydic H-shift to the peroxy group is consistent with
100 other carbonyl systems reported previously (Da Silva, 2011; Crouse et al., 2012; Møller et al.,
101 2016, 2019). Moreover, the kinetic modelling simulation on OH-initiated oxidation of hexanal
102 conducted by Barua et al. (2023) showed that a detectable concentration ($1.3 \times 10^4 \text{ molecules}$
103 cm^{-3}) of O₇ HOMs were produced even in the presence of 1 ppb NO. Because the non-
104 aldehydic H abstraction pathways are likely less prone to fragmentation and promote
105 functionalization, the effect of carbon chain length of *n*-aldehydes on HOM yields is of great
106 interest.

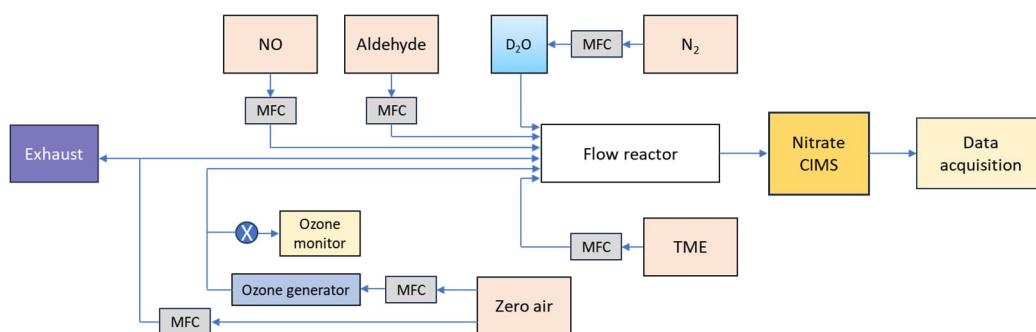
107 In this work, we experimentally studied the OH initiated autoxidation of C₅–C₈ *n*-
108 aldehydes in variable reaction times under atmospheric pressure and room temperature using
109 state-of-the-art mass spectrometry technique. In addition, the reactions were studied in the
110 presence of variable concentrations of NO to examine the effect of NO on the oxidation
111 process. The study shows how the length of carbon chain in linear aldehydes directly affects
112 the reactivity and functionalization of the molecules during their oxidation initiated by OH
113 radicals.

114 ■ METHODS

115 2.1 Experimental setup

116 The gas-phase oxidation reactions of *n*-aldehydes with OH radicals were conducted in a flow
117 reactor setup in the laboratory as shown in Fig. 1. All the experiments were conducted at room
118 temperature and 1 atm pressure of air. The precursor aldehydes were introduced into the reactor
119 from their individual gas cylinders. The oxidant OH radicals were produced in situ by the
120 reaction of tetramethylethylene (TME, C₆H₁₂) with ozone. We used an ozone generator that

121 photolyzes zero-air by a mercury lamp (UVP, Analytik Jena) to provide ozone to the reactor
 122 while TME was supplied from a gas cylinder. The zero-air was produced by feeding
 123 compressed clean air to a zero-air generator (AADCO-737-15) which was also used as bath
 124 gas in the reactor maintaining a total sample flow of 8–10 slpm. The initial concentrations of
 125 reactant precursors were determined by controlling the individual gas flows using calibrated
 126 mass flow controllers (Alicat Scientific). An ozone analyzer (2B Technologies model 205) was
 127 used to measure the ozone concentrations. Further details regarding reactant concentration
 128 measurements, as well as specifications for the chemicals and gas cylinders, are provided in
 129 Sects. S1 and S2 in the Supplement.



130

131 **Figure 1.** Schematic representation of a flow reactor setup showing a nitrate (NO_3^-) based
 132 chemical ionization mass spectrometer coupled to ambient pressure flow reactor. TME =
 133 tetramethylethylene (C_6H_{12}). The oxidant OH radical was produced in situ by TME + O_3
 134 reaction. MFC = mass flow controller.

135 We studied the reactions over a range of reaction times (short: 1–3 s, and long: 11–13
 136 s). The experimental conditions are presented in Table 1. Long reaction time experiments were
 137 conducted using a borosilicate flow reactor (length: 100 cm, and i.d.: 4.7 cm) while a quartz
 138 flow reactor (length: 100 cm, and i.d.: 2.2 cm) was used for the short reaction time experiments.
 139 We utilized the full volume of the reactor to achieve a long reaction time. However, the short
 140 reaction times were achieved by controlling the distance between the mass spectrometer orifice
 141 and the position where the precursor aldehyde meets the oxidant OH inside the reactor. This
 142 was done by using a movable injector that brings the aldehyde of interest at variable positions
 143 inside the reactor. The shortest possible reaction time of an individual aldehyde was chosen by
 144 the detection of any HOMs from its oxidation initiated by OH radicals. In short reaction time
 145 experiments, the highest concentration of VOC (6.4 ppmv) was used for pentanal while the
 146 concentrations of other aldehydes were up to 1 ppmv. The VOC concentrations of 0.2–2.5
 147 ppmv were used in long reaction time experiments. The other reactants including 43–97 ppbv

148 of TME, and 77–295 ppbv of ozone were maintained nearly constant with respect to individual
149 VOC in all experiment types (see Table 1). Among all the studied *n*-aldehyde systems, the
150 lowest level of aldehyde and O₃ concentrations were maintained for heptanal oxidation
151 experiment. This is because higher concentrations led to irrelevant products likely originating
152 from the ozonolysis of heptanal stabilizers (see Fig. S2 in the Supplement). To observe the
153 effect of NO_x on the OH induced oxidation of *n*-aldehydes, we conducted the experiments with
154 variable NO concentrations (2–1000 ppbv). Additionally, one more set of experiments,
155 hydrogen to deuterium (H/D) exchange, were conducted by the addition of D₂O flow to the *n*-
156 aldehyde OH oxidation reaction. These experiments give an estimate of the number of
157 functional groups with labile H atoms (e.g., OH, OOH, and C(O)OOH) in the oxidation
158 products. A near complete H/D conversion was confirmed by monitoring the reagent ion
159 signals of HNO₃NO₃⁻ and (HNO₃)₂NO₃⁻ fully converting to DNO₃NO₃⁻ and (DNO₃)₂NO₃⁻,
160 respectively (see Fig. S14 in the Supplement). The time series of reactive species, VOC, OH,
161 RO₂, O₃, and NO under different reaction conditions are shown in Figs. S16–S17 in the
162 Supplement.

163 The oxidation products were detected using a nitrate ion time-of-flight chemical
164 ionization mass spectrometer (NO₃⁻-ToF-CIMS) as their NO₃⁻ adducts. A zero-air sheath flow
165 of 20 slpm was provided to the chemical ionization inlet. The NO₃⁻ ions were produced from
166 gas-phase HNO₃ flow under soft X-ray exposure while being carried by N₂ to the inlet. The
167 mass spectrometric data processing, including averaging, baseline removal, mass axis
168 calibration, and peak integration were done using the tofTools v6.03 package for MATLAB.

169 **2.2 Kinetic simulation**

170 We estimated the concentrations of reactive species in the flow reactor during different *n*-
171 aldehyde oxidation experiments using a kinetic simulator Kinetiscope (version 1.1.1136.x64)
172 (Hinsberg and Houle, 2022). These include the average concentrations of OH radicals and
173 initial RO₂ radicals (i.e., C_nH_{2n-1}O₃, the first peroxy radicals formed in the oxidation process)
174 produced in the experiments. In the simulations, a single-reactor model with constant volume,
175 pressure, and temperature was employed. The temperature was set to 298.15 K. The simulation
176 setting parameters such as total number of particles (1 × 10⁹) and random number seed
177 (12947) were kept constant for consistency, while the maximum simulation time was matched
178 to that of individual experiments. Details of all the simulations are provided in Sect. S13 in the
179 Supplement.

180 **Table 1.** The experimental conditions for OH initiated oxidation of studied C₅–C₈ *n*-aldehydes.

Experiment type	[VOC] ^Φ	[TME] ^Φ	[O ₃] ^Φ	[OH] ^{Φ‡}	[NO] ^Φ	D ₂ O	Δt [‡]
VOC	ppmv	ppbv	ppbv	pptv	ppbv	y/n [±]	s
Short residence time							
Pentanal (C ₅ H ₁₀ O)	6.4	48.2	295	4.4	N/A [†]	n	2.3
Hexanal (C ₆ H ₁₂ O)	1.0	43.2	225	3.4	N/A	n	1.1, 2.9
Octanal (C ₈ H ₁₆ O)	0.72	48.2	208	3.1	N/A	n	1.0, 2.1
Long residence time							
Pentanal (C ₅ H ₁₀ O)	2.5	48.2	295	4.4	N/A	n	12.8
Hexanal (C ₆ H ₁₂ O)	1.0	43.2	225	3.4	N/A	n	11.5
Heptanal (C ₇ H ₁₄ O)	0.15	96.5	77	1.2	N/A	n	12.8
Octanal (C ₈ H ₁₆ O)	0.72	48.2	208	3.1	N/A	n	12.8
Experiments with NO							
Pentanal (C ₅ H ₁₀ O)	1.3	48.2	208	3.1	2–1000	n	12.8
Hexanal (C ₆ H ₁₂ O)	1.0	43.2	225	3.4	2–200	n	11.5
Octanal (C ₈ H ₁₆ O)	0.72	48.2	208	3.1	2–1000	n	12.8
Experiments with D₂O							
Pentanal (C ₅ H ₁₀ O)	2.5	48.2	295	4.4	N/A	y	12.8
Hexanal (C ₆ H ₁₂ O)	1.0	43.2	225	3.4	N/A	y	11.5
Heptanal (C ₇ H ₁₄ O)	0.10	96.5	77	1.2	N/A	y	12.8
Octanal (C ₈ H ₁₆ O)	0.72	48.2	208	3.1	N/A	y	12.8

181 ^Φ Initial reactant concentrations.

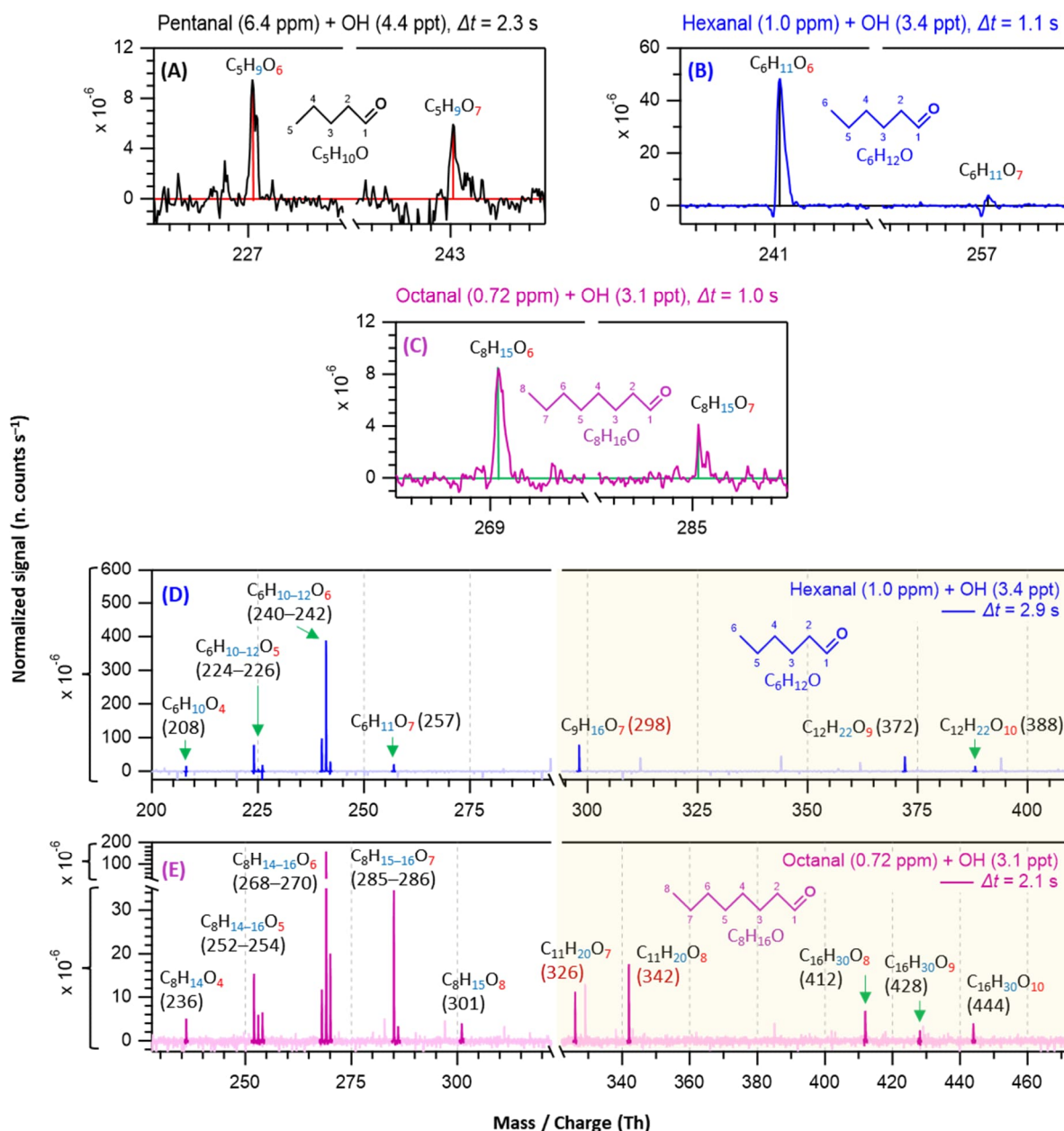
182 [‡] The initial OH concentrations were calculated using bimolecular rate coefficients $k_{O_3-TME} =$
 183 $1.5 \times 10^{-15} \text{ cm}^3 \text{ s}^{-1}$, $k_{OH-TME} = 1.0 \times 10^{-10} \text{ cm}^3 \text{ s}^{-1}$ (Manion et al., 2015), and the expression
 184 $[OH] = (k_{O_3-TME} * [O_3]) / k_{OH-TME}$.

185 [†] Not applicable (N/A). [±] D₂O added = y, not added = n. [‡] Reaction time (Δt).

186 ■ RESULTS AND DISCUSSION

187 3.1 Detection of HOM in short to long reaction time experiments

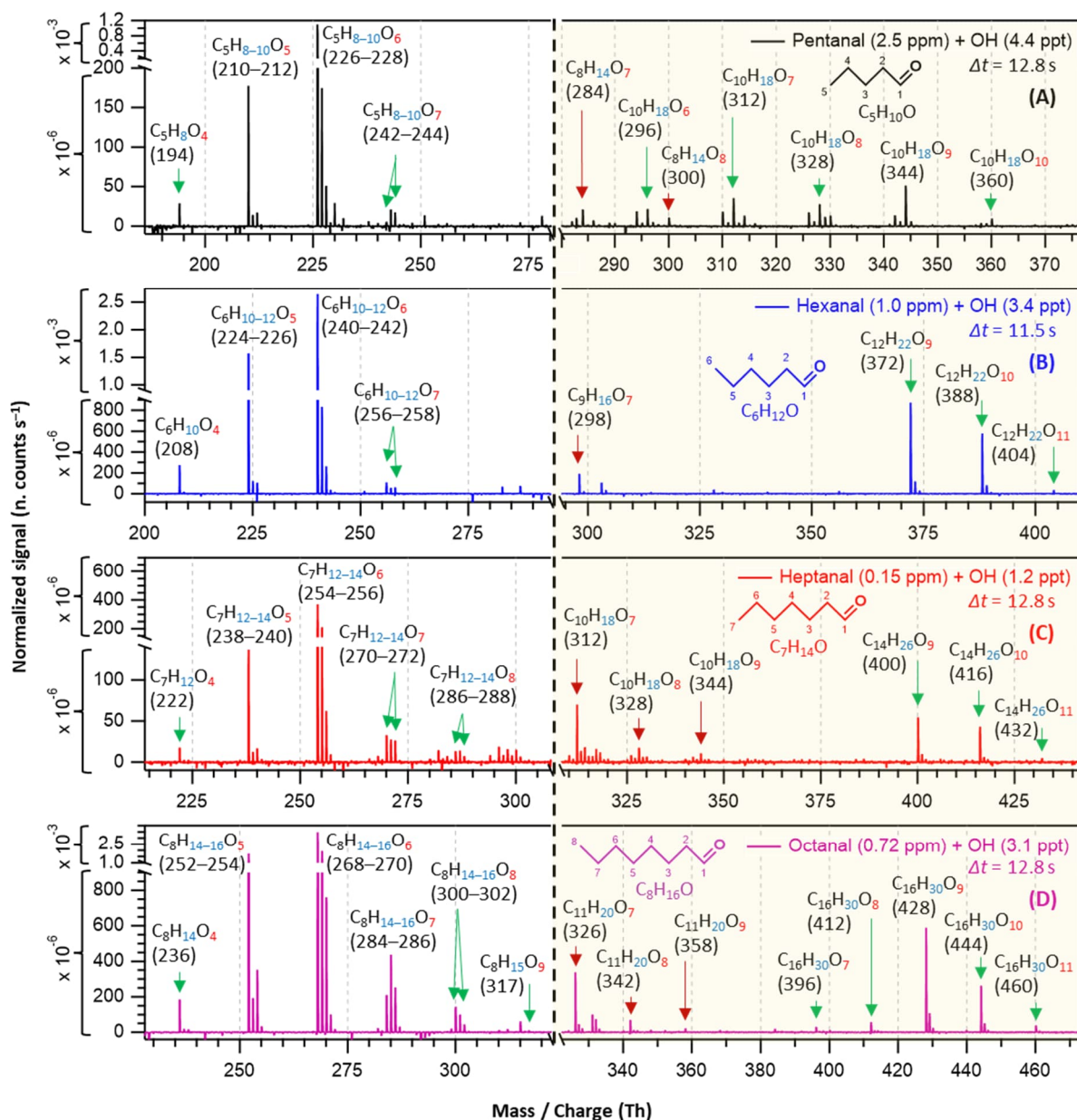
188 In this section, we discuss how early HOMs formed and how they evolved with the progress
189 of reaction time in different *n*-aldehyde OH oxidation experiments. The hexanal OH oxidation
190 spectra included in Figs. 2–3 are reproduced from our previous study (Barua et al., 2023) for
191 comparison with the other aldehydes. Figure 2 shows the results from short reaction time ($\Delta t =$
192 1–3 s) experiments. We observed the formation of O₆ and O₇ HOMs within 1.0, 1.1, and 2.3 s
193 reaction times in the oxidation experiments of octanal, hexanal, and pentanal, respectively. It
194 is essential to mention that with the increase of number of carbon atoms in the studied
195 aldehydes, the required precursor concentrations for first HOM observation decreased (from
196 6.4 ppm pentanal, 1 ppm hexanal to 0.72 ppm octanal; corresponding reacted concentrations
197 1.15, 0.34, and 0.30 ppb, respectively). This shows a clear effect of carbon chain length on the
198 reactivity of linear aldehydes towards HOM formation. Because the oxidation process of *n*-
199 aldehydes (C_nH_{2n}O) with OH is initiated by the abstraction of a H atom (aldehydic or non-
200 aldehydic), the first formed acyl (or alkyl) peroxy radical C_nH_{2n-1}O₃ contains an odd number
201 of oxygen atoms. If autoxidation outcompetes any other bimolecular reactions (e.g., RO₂ +
202 RO₂, RO₂ + HO₂, etc.), the product spectrum will be mostly dominated by odd number of
203 oxygen containing products. In all studied *n*-aldehyde systems, the intensity of O₆ HOM is
204 higher than that of O₇ HOM (Figs. 2–3). The formation of C_nH_{2n-1}O₆ peroxy radical indicates
205 that the process certainly involves a bimolecular reaction step. In hexanal OH oxidation, Barua
206 et al. (2023) computationally showed that the formation of C₆H₁₁O₅ peroxy radical via
207 autoxidation is very fast while the subsequent isomerization reaction leading to C₆H₁₁O₇ is
208 slower. The same is likely to hold true for other aldehydes and it is expected that the C_nH_{2n-1}O₅
209 peroxy radical undergoes a bimolecular reaction converting it to C_nH_{2n-1}O₄ alkoxy radical,
210 followed by a H-shift, and subsequent O₂ addition reactions producing the dominant C_nH_{2n-1}O₆
211 HOM (see Figs. S7–S11 in the Supplement). As the reaction time increased, we observed the
212 formation of monomeric HOM up to O₇ and accretion products up to O₁₀ composition within
213 2.9 s in hexanal oxidation (see Fig. 2D) with the consumption of $\sim 8.88 \times 10^{-4}$ of its initial
214 concentration. In the case of octanal, monomeric O₈ HOM and accretion products up to O₁₀
215 formed within 2.1 s reaction time (see Fig. 2E) with a comparable reacted fraction
216 ($\sim 8.71 \times 10^{-4}$) of its initial concentration.



217

218 **Figure 2.** Nitrate chemical ionization mass spectra of OH initiated oxidation of *n*-aldehydes
 219 showing the formation of HOMs in different reaction times (Δt): 2.3 s – pentanal in black (A),
 220 1.1 and 2.9 s – hexanal in blue (B and D), and 1.0 and 2.1 s – octanal in purple (C and E). The
 221 product peaks are labelled with the exclusion of NO_3^- ion attachment in their compositions.
 222 The backgrounds of TME ozonolysis (TME + O_3) and aldehyde have been subtracted from all
 223 spectra, resulting in several negative peaks in panels A–E. The accretion product region is
 224 highlighted in light gold background. The accretion products labeled with nominal mass/charge
 225 in dark red ($\text{C}_{n+3}\text{H}_{2n+4}\text{O}_{7-8}$) are related to the TME-derived peroxy radical $\text{C}_3\text{H}_5\text{O}_3$.

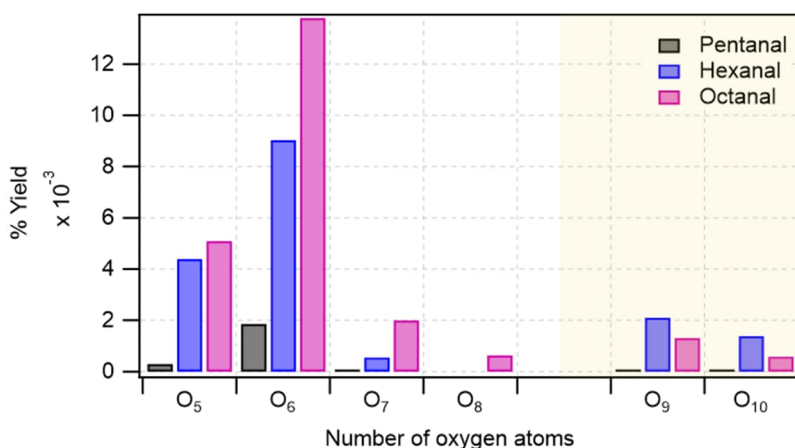
226 In long reaction time (11–13 s) experiments, we observed higher intensities of product
227 signals (see Fig. 3) in comparison to their intensities in the short reaction time experiments - as
228 expected. For pentanal, Fig. 3A shows that HOM accretion products up to O₁₀ formed within
229 12.8 s reaction time which were not seen in the short reaction time experiment (2.3 s). A lower
230 precursor concentration, 2.5 ppm of pentanal in long reaction time experiment compared to
231 earlier 6.4 ppm in short reaction time, was sufficient to produce the observed HOMs in this
232 case. A close observation of C₆–C₈ *n*-aldehyde oxidation spectra (Fig. 3B–D) reveals that HOM
233 accretion products up to O₁₁ formed within 11–13 s reaction time under the experimental
234 conditions. In all *n*-aldehyde experiments, we also observed the accretion products resulting
235 from different combinations of aldehyde-derived peroxy radicals C_nH_{2n-1}O₆₋₈ and TME-
236 derived peroxy radical C₃H₅O₃ (see Fig. S13 in the Supplement for details) which are marked
237 with dark red arrows. Figure 3D implies that the highest oxygenation (C₈H₁₅O₉) in the
238 monomeric HOM products is associated with octanal, whereas Fig. 3C shows that the most
239 oxygenated products produced from heptanal are C₇H₁₂₋₁₄O₈. In the case of pentanal and
240 hexanal, monomeric HOMs are limited to seven oxygen atoms (see Fig. 3A–B). All in all, we
241 notice a near identical distribution of oxidation products in the experiments with all C₅–C₈ *n*-
242 aldehydes. However, the tendency of oxidation gets faster and advances to higher oxygenated
243 products when the carbon chain length increases.



244

245 **Figure 3.** Nitrate chemical ionization mass spectra of OH initiated oxidation of *n*-aldehydes in
 246 11–13 s residence times: pentanal in black (A), hexanal in blue (B), heptanal in red (C), and
 247 octanal in purple (D). The product peaks are labelled with the exclusion of NO_3^- ion attachment
 248 in their compositions. The backgrounds of TME ozonolysis ($\text{TME} + \text{O}_3$) and aldehyde have
 249 been subtracted from all spectra, resulting in several negative peaks in panels A–D. The
 250 accretion product region is highlighted in light gold background. The accretion products
 251 marked by dark red arrows ($\text{C}_{n+3}\text{H}_{2n+4}\text{O}_{7-9}$) are related to the TME-derived peroxy radical
 252 $\text{C}_3\text{H}_5\text{O}_3$.

253 The bar plot (see Fig. 4) compares the yields of major oxidation products from different
 254 *n*-aldehydes. It clearly shows that the yields of higher oxygenated products increase as we move
 255 from pentanal to octanal. In the accretion product regime, the yields of O₉–O₁₀ products in
 256 octanal are lower than that of hexanal which is also reflected in their dimer to monomer ratios
 257 with octanal being 8.8×10^{-2} and hexanal being 2.5×10^{-1} . The lower ratio for octanal
 258 compared to hexanal is observed despite both precursors producing comparable quantities of
 259 initial RO₂ radicals (9.12×10^9 and 9.37×10^9 molecules cm⁻³ from octanal and hexanal,
 260 respectively; see Table S1 in the Supplement). This can lie in the variation of RO₂ + RO₂
 261 reaction rate coefficients forming the accretion products (RO₂ + RO₂ → ROOR + O₂) which is
 262 highly dependent on specific RO₂ structures (Shallcross et al., 2005; Berndt et al., 2018).

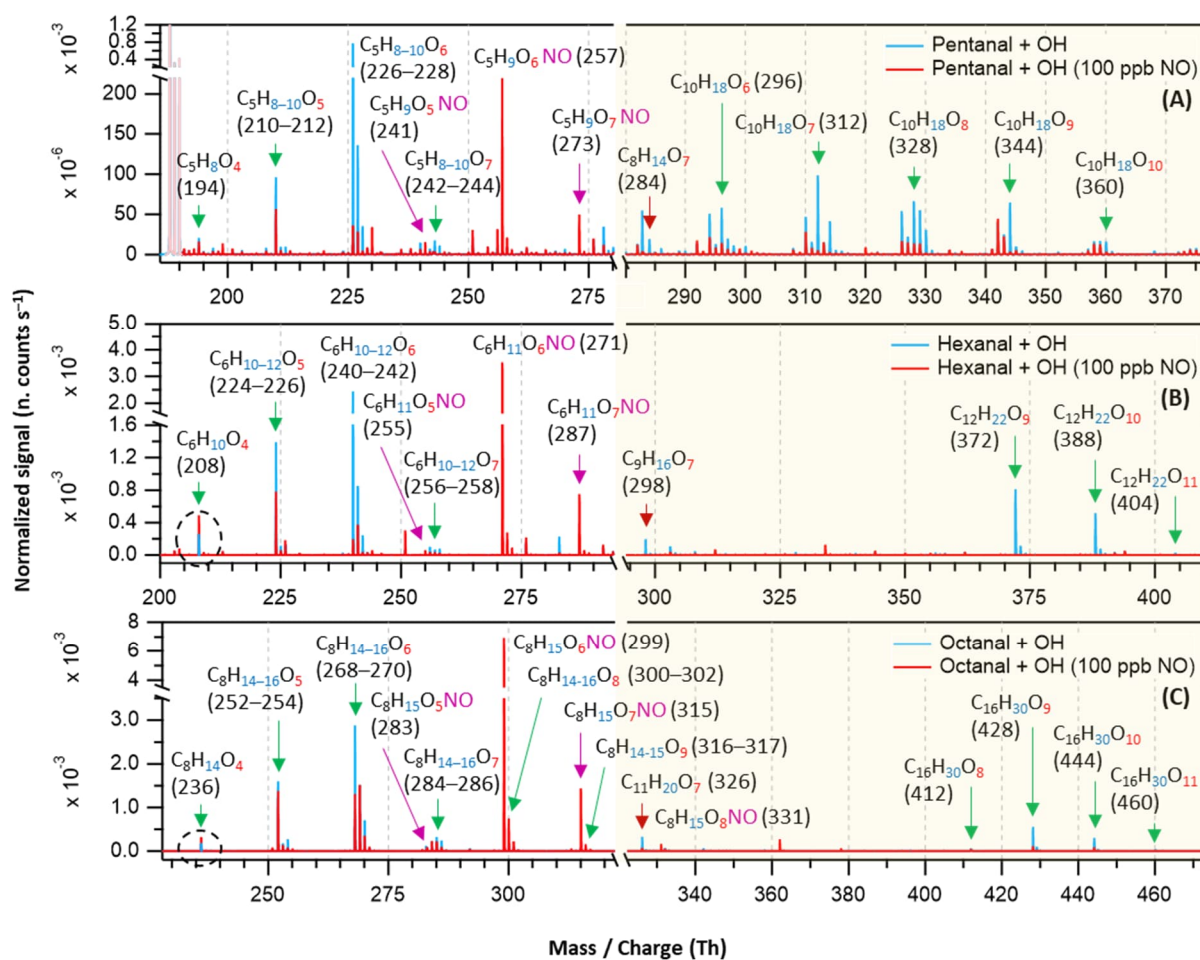


263
 264 **Figure 4.** Distribution of major oxidation products (O₅–O₈ in monomeric regime with white
 265 background, and O₉–O₁₀ in accretion product regime with light gold background) in pentanal,
 266 hexanal, and octanal oxidation initiated by OH radical. In y-axis, the numbers are the
 267 cumulative sum of yields of products with the same oxygen number. Reaction time, $\Delta t = 11$ –
 268 13 s.

269 3.2 Experiments in the presence of NO

270 It has been widely acknowledged that the formation of HOM is suppressed in high NO_x
 271 conditions (Wildt et al., 2014; Praske et al., 2018; McFiggans et al., 2019; Pullinen et al., 2020),
 272 thus reducing the SOA yields. In this process, the reduction in SOA yield is largely attributed
 273 to the suppression of highly condensable HOM accretion products (RO₂ + RO₂ → ROOR)
 274 (Kirkby et al., 2016; Pullinen et al., 2020). However, other studies have shown that NO can
 275 also enhance HOM formation by producing reactive RO radicals (RO₂ + NO → RO + NO₂)
 276 that can propagate autoxidation (Rissanen, 2018; Yan et al., 2020; Wang et al., 2021; Shen et
 277 al., 2022; Nie et al., 2023; Barua et al., 2025; Kang et al., 2025). In our different *n*-aldehyde

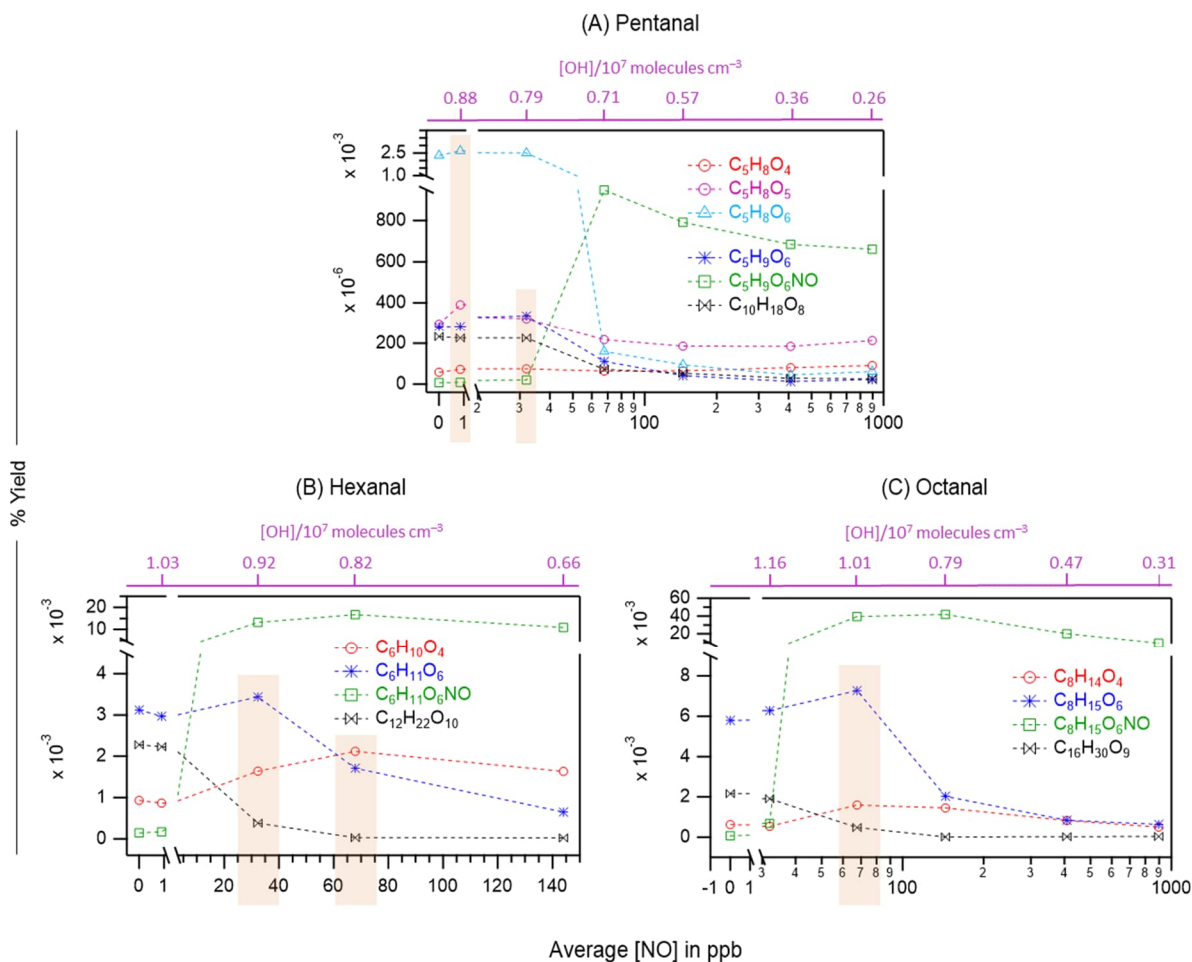
278 oxidation experiments in the presence of variable concentrations of NO, we observed the
 279 general tendency of dropping of the accretion product signals ($C_{2n}H_{4n-2}O_z$) and their
 280 corresponding yields as expected (see Figs. 5 and 6). Figure 5 represents the mass spectra
 281 recorded in the experiments without (in blue) and with the presence of 100 ppb initial NO (in
 282 red). At this condition, most of the monomeric products are quenched at different extents
 283 alongside the formation of organonitrates while the accretion products are quenched nearly
 284 completely. Interestingly, we observed some enhancement in the intensities of O_4 products in
 285 the case of hexanal and octanal (Fig. 5B–C) under 100 ppb NO. A closer look at Fig. 6A reveals
 286 that the yields of closed-shell products $C_5H_8O_{4-6}$ somewhat increased under around 1 ppb
 287 average NO condition which then started to decrease under higher NO of around 30 ppb and
 288 above in pentanal oxidation. In both pentanal and hexanal oxidations, the dominant O_6 peroxy
 289 radicals ($C_5H_9O_6$ and $C_6H_{11}O_6$ respectively, blue markers) gained higher yields under around
 290 30 ppb of NO (Fig. 6A–B) compared to without NO condition.



291
 292 **Figure 5.** Overlaid nitrate chemical ionization mass spectra of OH initiated oxidation of *n*-
 293 aldehydes without (in blue) and with the presence of 100 ppb of initial NO (in red): pentanal

294 (A), hexanal (B), and octanal (C). The product peaks are labelled with the exclusion of NO_3^-
 295 ion attachment in their compositions. The accretion product region is highlighted in light gold
 296 background. The accretion products marked by dark red arrows ($\text{C}_{n+3}\text{H}_{2n+4}\text{O}_{7-9}$) are related to
 297 the TME-derived peroxy radical $\text{C}_3\text{H}_5\text{O}_3$. The organonitrates (in the presence of NO) are
 298 labelled with the extension NO and marked with purple arrows. Reaction time, $\Delta t = 11\text{--}13$ s.

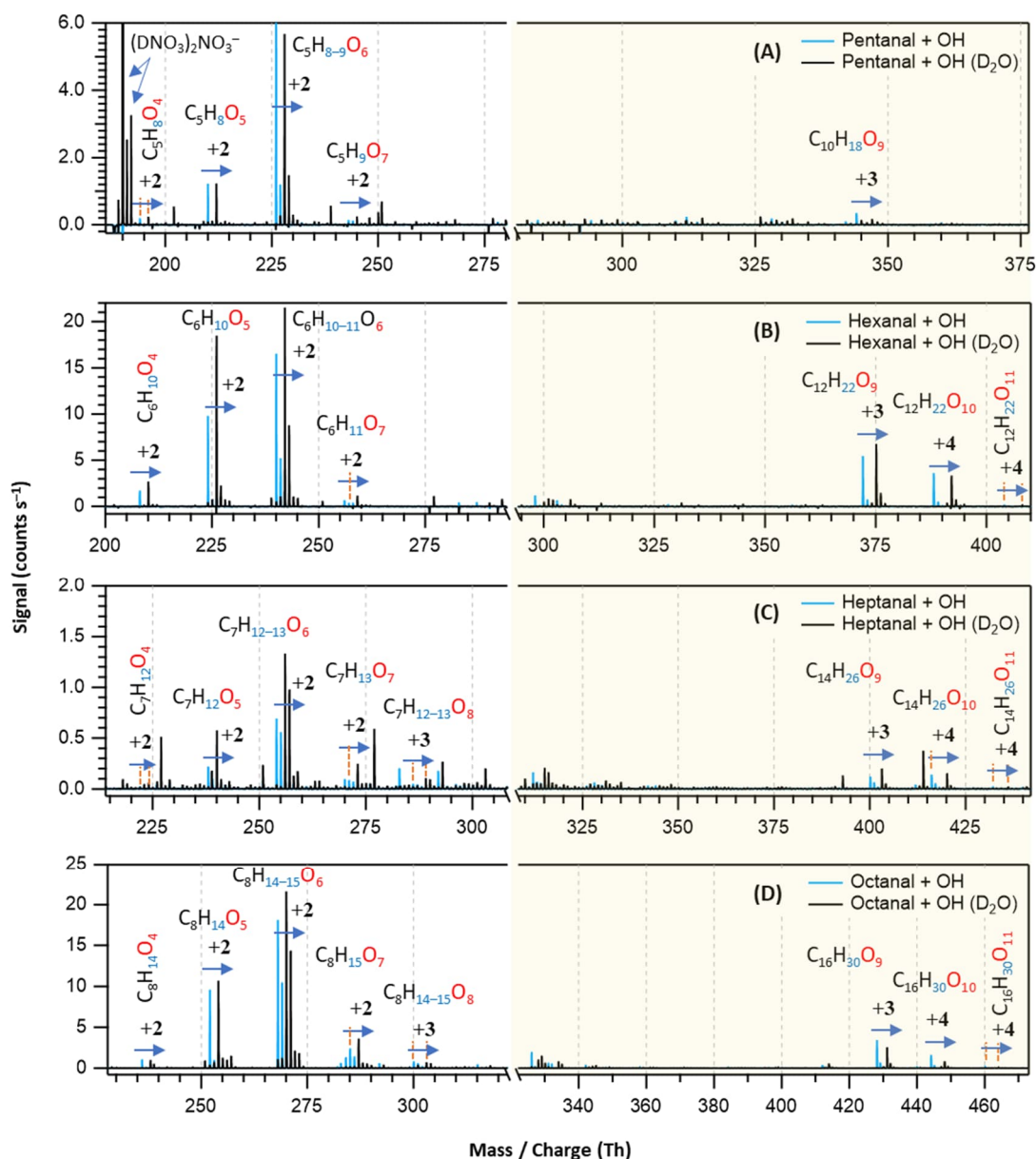
299 On the other hand, in octanal oxidation, the yield of dominant O_6 peroxy radical ($\text{C}_8\text{H}_{15}\text{O}_6$)
 300 increased even under 70 ppb of NO (see Fig. 6C). These observations indicate that the
 301 suppressing effect of NO on the yields of HOMs in *n*-aldehyde oxidation is perturbed with the
 302 increase of carbon chain length of the precursor aldehyde. Also, in all the studied *n*-aldehydes,
 303 although highly oxygenated products are suppressed under higher NO concentrations, we see
 304 some enhancement in the early oxygenated closed shell products ($\text{O}_4\text{--}\text{O}_5$, and even O_6 product
 305 in pentanal) under relatively lower NO concentrations. It should be noted that the formation of
 306 organonitrates with chemical composition $\text{C}_n\text{H}_{2n-1}\text{O}_z\text{NO}$ strongly supports our assignment of
 307 reactive peroxy radical intermediates $\text{C}_n\text{H}_{2n-1}\text{O}_z$. Additional insights into the abundance of
 308 HOMs under varying NO concentrations are discussed in Sect. S12 in the Supplement.



310 **Figure 6.** The yields of different oxidation products including monomeric HOMs,
311 organonitrates (green markers), and HOM accretion products (black markers) as a function of
312 average NO concentrations in OH initiated oxidation of *n*-aldehydes: pentanal (A), hexanal
313 (B), and octanal (C). The corresponding average OH radical concentrations in these
314 experiments are shown with purple scales. Note the logarithmic scale (x-axis) in panels A and
315 C. The orange rectangles highlight the enhanced yields of several non-nitrogen containing
316 products: O₄–O₆ closed-shell products from pentanal under around 1 ppb NO (A), O₄ closed-
317 shell products from hexanal and octanal under around 70 ppb NO (B and C), O₆ peroxy radical
318 from pentanal and hexanal under around 30 ppb NO (A and B) and the same from octanal under
319 70 ppb NO (C). Reaction time, $\Delta t = 11\text{--}13$ s.

320 **3.3 D₂O experiments**

321 With the addition of D₂O in the OH initiated oxidation experiments of *n*-aldehydes, we
322 observed a shift in individual product signals in the mass spectra equivalent to the number of
323 exchangeable H atoms in the product structures (see Fig. 7). This provides additional insight
324 into the product identities in terms of the total number of OH, OOH, and (or) C(O)OOH groups
325 present in their molecular structures. Figure 7 shows that the oxidation products with same
326 number of oxygen atoms in all the studied *n*-aldehydes undergo identical mass shifts (H/D
327 exchange) in the presence of D₂O. This observation indicates that the autoxidation mechanism
328 derived by Barua et al. (2023) for hexanal OH oxidation (see Fig. S5 in the Supplement) is
329 directly applicable to the other linear aldehydes studied here and thus produces similar product
330 structures. The original mechanism is extended to HOMs up to nine oxygen atoms and
331 presented in Fig. S6 in the Supplement. The likely formation process of HOM accretion
332 products (C_{2n}H_{4n-2}O₉₋₁₁) is shown in Fig. S12 in the Supplement. The proposed structures of
333 O₅ closed-shell products, O₆–O₈ monomeric HOMs as well as O₉₋₁₁ HOM accretion products
334 (see Figs. S6–S12 in the Supplement) agree with the H/D exchange experiments in terms of
335 their 2–4 units of mass shifts in the respective *n*-aldehyde mass spectra (see Fig. 7).



336

337 **Figure 7.** Overlaid nitrate chemical ionization mass spectra of OH initiated oxidation of *n*-
 338 aldehydes without (in blue) and with the presence of D₂O (in black): pentanal (A), hexanal (B),
 339 heptanal (C), and octanal (D). In panel (A), the label (DNO₃)₂NO₃⁻ is assigned to the deuterated
 340 nitric acid trimer reagent signal. The product peaks are labelled with the exclusion of NO₃⁻ ion
 341 attachment in their compositions and the numbers on the blue arrows indicate the individual
 342 counts of mass shift during H/D exchange. The backgrounds of TME ozonolysis (TME + O₃)
 343 and aldehyde have been subtracted from the spectra, resulting in several negative peaks in
 344 panels A–B. The accretion product region is highlighted in light gold background.

345 **3.4 Atmospheric implications**

346 Ambient concentration of individual longer chain aldehyde ($\geq C_5$) can vary from sub-ppb to
347 several ppb depending on time and location (Williams et al., 1996; Duan et al., 2008; Li et al.,
348 2018; Ma et al., 2019). A total concentration of C_6 – C_{10} *n*-aldehydes in Monti Cimino Forest in
349 Italy was measured to be 8.8 ppb (Ciccioli et al., 1993). In indoor air, the concentration can be
350 significantly higher, even around 50 ppb (Birmili et al., 2022). Atmospheric lifetime of *n*-
351 aldehydes due to their reactivity with OH radicals is generally less than 10 h (Albaladejo et al.,
352 2002; Aguirre et al., 2025). Because of their significant photochemical ozone formation
353 potential (Jenkin et al., 2017; Aguirre et al., 2025), they are good candidates for generating
354 photochemical smog in NO_x rich polluted urban atmosphere. On the other hand, previous
355 studies have shown that atmospheric oxidation products of longer chain *n*-aldehydes are direct
356 contributors to the formation of SOA (Chacon-Madrid et al., 2010; Fan et al., 2024). Here, we
357 demonstrated that the studied C_5 – C_8 *n*-aldehydes can rapidly form HOM via autoxidation
358 initiated by OH radicals, and the length of carbon chain controls the efficiency of the process.
359 Therefore, with the increase of carbon chain length in *n*-aldehydes, the fast formation of HOMs
360 is expected to take part in the early stages of gas-to-particle formation and growth contributing
361 to atmospheric SOA. Our experiments in the presence of NO showed a general decreasing trend
362 of HOM accretion products with increasing NO but also formed the corresponding highly
363 oxygenated organic nitrates (HOM-ONs). In our study with the *n*-aldehydes under 1–70 ppb
364 NO conditions, some yield enhancement with oxidation products up to six O atoms was also
365 seen. Pullinen et al. (2020) showed that both HOMs and HOM-ONs originated from the same
366 peroxy radicals with more than six O atoms condensed on particles by about 50% and those
367 with more than eight O atoms condensed by about 100% to form SOA in monoterpene
368 photooxidation. Moreover, other reports show that HOM-ONs originated from different VOCs
369 can contribute to low volatility products (Barua et al., 2025) and thereby particle growth and
370 aerosol mass loading (Fry et al., 2014; Lee et al., 2016; Huang et al., 2019).

371 **■ CONCLUSIONS**

372 This study represents the significance of longer chain linear aldehydes ($\geq C_5$), key components
373 of atmospherically abundant oxygenated volatile organic compounds (OVOCs), in rapid
374 formation of HOMs upon atmospheric oxidation and their potential contribution to atmospheric
375 SOA. Among the studied C_5 – C_8 *n*-aldehydes, the fastest HOM formation is associated with
376 octanal forming O_6 and O_7 HOMs within 1.0 s reaction time with low precursor loading.

377 Pentanal and hexanal formed HOMs with the same number of oxygen atoms as early as 2.3
378 and 1.1 s, respectively but with higher precursor loadings (i.e., 6.4 ppm pentanal and 1.0 ppm
379 hexanal compared to 0.72 ppm octanal). The highest oxygenated monomeric HOM with 9
380 oxygen atoms was formed from octanal whereas the numbers are up to 8 oxygen atoms for
381 heptanal and 7 oxygen atoms for both pentanal and hexanal oxidation initiated by OH radicals
382 within 13 s reaction time. Although the highest precursor concentration (6.4 ppm) was required
383 for the first observation of detectable HOM in short reaction time experiment with pentanal, a
384 lower concentration (2.5 ppm) was used to obtain its observed mass spectrum in the long
385 reaction experiment. The HOM accretion products with up to 11 oxygen atoms were observed
386 in C₆–C₈ *n*-aldehyde oxidation experiments while they were limited to maximum 10 oxygen
387 atoms in pentanal case. We also observed the trend of increased oxidation product yields with
388 the increase of carbon chain length. In all studied systems, the dominant product signals are O₆
389 HOMs with the O₅ HOMs being the second dominant ones. Previous mechanistic
390 understanding (Barua et al., 2023) as well as current experimental observations reveal that
391 autoxidation process forming O₅ RO₂ in *n*-aldehydes is very fast while the subsequent
392 unimolecular rearrangements of the RO₂ intermediates are in competition with bimolecular
393 reactions including other RO₂, HO₂, and NO_x. The experiments in the presence of high NO
394 concentrations (30 ppb and above) produced the highest yields of HOM-ONs, compared to
395 neighboring non-nitrogen HOMs, with the expense of HOM accretion products. However,
396 some enhancements with the yields of low oxygenated closed-shell products and O₆ peroxy
397 radicals were also seen under 1–70 ppb NO conditions. The results of hydrogen to deuterium
398 (H/D) exchange experiments with identical mass shifts in the oxidation products of all studied
399 *n*-aldehydes imply that the autoxidation mechanism established for hexanal (Barua et al., 2023)
400 is valid for other *n*-aldehydes. Therefore, accounting for linear aldehydes and their atmospheric
401 oxidation with increasing importance to longer carbon chain length as a direct source of
402 condensable materials even under moderately polluted urban areas is essential.

403 ■ DATA AVAILABILITY

404 Details about the experimental setup and mass spectrometry, chemicals and gas cylinders,
405 mechanistic details of the oxidation steps, additional insights into abundance of HOMs, and
406 details of kinetic simulations are provided in the Supplement. An Excel file (.xlsx) with results
407 from mass spectrometry, and two example Kinetiscope (.rxn) files containing kinetic
408 simulation input parameters—one with NO, another without—are available online
409 (<https://doi.org/10.5281/zenodo.18894230>; Barua, 2026).

410 ■ **AUTHOR CONTRIBUTIONS**

411 Conceptualization: MR, SB, AK; data curation: SB, AK; formal analysis: SB; investigation:
412 SB, AK, PS, SI, MR; methodology: SB, AK; writing (original draft preparation): SB; writing
413 (review and editing): SB, AK, PS, SI, MR; funding acquisition: SI, MR.

414 ■ **COMPETING INTERESTS**

415 The authors declare that they have no conflict of interest.

416 ■ **ACKNOWLEDGEMENTS**

417 This project has received funding from the European Research Council under the European
418 Union's Horizon 2020 research and innovation programme under Grant No. 101002728 (ERC
419 Consolidator Grant Project ADAPT) and from the European Union's horizon Europe research
420 and innovation programme under Grant No. 101096133 (PAREMPI: particle emission
421 prevention and impact: from real-world emissions of traffic to secondary PM of 585 urban air).
422 The support from the Research Council of Finland (331207, 336531, 346373, 347775, 353836,
423 and 355966) and Doctoral school of the Faculty of Engineering and Natural Sciences of
424 Tampere University are greatly appreciated. We thank the tofTools team for providing the data
425 analysis program.

426 ■ **REFERENCES**

- 427 Aguirre, F., Lugo G, P. L., Straccia C, V. G., Teruel, M. A., and Blanco, M. B.: Atmospheric oxidation of long
428 chain aldehydes: OH and Cl reactivity, mechanisms and environmental impact, *Atmos. Environ.*, 360,
429 121429, <https://doi.org/10.1016/j.atmosenv.2025.121429>, 2025.
- 430 Albaladejo, J., Ballesteros, B., Jiménez, E., Martín, P., and Martínez, E.: A PLP-LIF kinetic study of the
431 atmospheric reactivity of a series of C4–C7 saturated and unsaturated aliphatic aldehydes with OH,
432 *Atmos. Environ.*, 36(20), 3231–3239, [https://doi.org/10.1016/S1352-2310\(02\)00323-0](https://doi.org/10.1016/S1352-2310(02)00323-0), 2002.
- 433 Barua, S.: Rapid formation of secondary aerosol precursors from the autoxidation of C₅–C₈ n-aldehydes, Zenodo
434 [data set], <https://doi.org/10.5281/zenodo.18894230>, 2026.
- 435 Barua, S., Iyer, S., Kumar, A., Seal, P., and Rissanen, M.: An aldehyde as a rapid source of secondary aerosol
436 precursors: Theoretical and experimental study of hexanal autoxidation, *Atmos. Chem. Phys.*, 23(18),
437 10517–10532, <https://doi.org/10.5194/acp-23-10517-2023>, 2023.

438 Barua, S., Kumar, A., Seal, P., Bezaatpour, M., Jha, S., Myllys, N., Iyer, S., and Rissanen, M.: Rapid formation
439 of aerosol precursors from the autoxidation of aromatic carbonyls and the remarkable enhancing
440 influence of NO addition, *Research Square* [preprint], <https://doi.org/10.21203/rs.3.rs-7332278/v1>, 28
441 August 2025.

442 Berndt, T., Richters, S., Jokinen, T., Hyttinen, N., Kurtén, T., Otkjær, R. V., Kjaergaard, H. G., Stratmann, F.,
443 Herrmann, H., Sipilä, M., Kulmala, M., and Ehn, M.: Hydroxyl radical-induced formation of highly
444 oxidized organic compounds, *Nat. Commun.*, 7(1), 13677, <https://doi.org/10.1038/ncomms13677>,
445 2016.

446 Berndt, T., Richters, S., Kaethner, R., Voigtländer, J., Stratmann, F., Sipilä, M., Kulmala, M., and Herrmann,
447 H.: Gas-Phase Ozonolysis of Cycloalkenes: Formation of Highly Oxidized RO₂ Radicals and Their
448 Reactions with NO, NO₂, SO₂, and Other RO₂ Radicals, *J. Phys. Chem. A*, 119(41), 10336–10348,
449 <https://doi.org/10.1021/acs.jpca.5b07295>, 2015.

450 Berndt, T., Scholz, W., Mentler, B., Fischer, L., Herrmann, H., Kulmala, M., and Hansel, A.: Accretion Product
451 Formation from Self- and Cross-Reactions of RO₂ Radicals in the Atmosphere, *Angew. Chem. Int.*
452 *Edit.*, 57(14), 3820–3824, <https://doi.org/10.1002/anie.201710989>, 2018.

453 Bianchi, F., Kurtén, T., Riva, M., Mohr, C., Rissanen, M. P., Roldin, P., Berndt, T., Crouse, J. D., Wennberg,
454 P. O., Mentel, T. F., Wildt, J., Junninen, H., Jokinen, T., Kulmala, M., Worsnop, D. R., Thornton, J. A.,
455 Donahue, N., Kjaergaard, H. G., and Ehn, M.: Highly Oxygenated Organic Molecules (HOM) from
456 Gas-Phase Autoxidation Involving Peroxy Radicals: A Key Contributor to Atmospheric Aerosol,
457 *Chem. Rev.*, 119(6), 3472–3509, <https://doi.org/10.1021/acs.chemrev.8b00395>, 2019.

458 Birmili, W., Daniels, A., Bethke, R., Schechner, N., Brasse, G., Conrad, A., Kolossa-Gehring, M., Debiak, M.,
459 Hurraß, J., Uhde, E., Omelan, A., and Salthammer, T.: Formaldehyde, aliphatic aldehydes (C₂-C₁₁),
460 furfural, and benzaldehyde in the residential indoor air of children and adolescents during the German
461 Environmental Survey 2014–2017 (GerES V), *Indoor Air*, 32(1), <https://doi.org/10.1111/ina.12927>,
462 2022.

463 Brean, J., Beddows, D. C. S., Shi, Z., Temime-Roussel, B., Marchand, N., Querol, X., Alastuey, A., Minguillón,
464 M. C., and Harrison, R. M.: Molecular insights into new particle formation in Barcelona, Spain, *Atmos.*
465 *Chem. Phys.*, 20(16), 10029–10045, <https://doi.org/10.5194/acp-20-10029-2020>, 2020.

466 Brean, J., Harrison, R. M., Shi, Z., Beddows, D. C. S., Acton, W. J. F., Hewitt, C. N., Squires, F. A., and Lee, J.:
467 Observations of highly oxidized molecules and particle nucleation in the atmosphere of Beijing,
468 Atmos. Chem. Phys., 19(23), 14933–14947, <https://doi.org/10.5194/acp-19-14933-2019>, 2019.

469 Calogirou, A., Larsen, B. R., and Kotzias, D.: Gas-phase terpene oxidation products: A review, Atmos.
470 Environ., 33(9), 1423–1439, [https://doi.org/10.1016/S1352-2310\(98\)00277-5](https://doi.org/10.1016/S1352-2310(98)00277-5), 1999.

471 Calvert, J., Mellouki, A., Orlando, J., Pilling, M., and Wallington, T.: Mechanisms of Atmospheric Oxidation of
472 the Oxygenates, Oxford University Press, USA, <https://doi.org/10.1093/oso/9780199767076.001.0001>,
473 2011.

474 Carlier, P., Hannachi, H., and Mouvier, G.: The chemistry of carbonyl compounds in the atmosphere—A
475 review, Atmos. Environ., 20(11), 2079–2099, [https://doi.org/10.1016/0004-6981\(86\)90304-5](https://doi.org/10.1016/0004-6981(86)90304-5), 1986.

476 Cassanelli, P., Johnson, D., and Anthony Cox, R.: A temperature-dependent relative-rate study of the OH
477 initiated oxidation of n-butane: The kinetics of the reactions of the 1- and 2-butoxy radicals, Phys.
478 Chem. Chem. Phys., 7(21), 3702, <https://doi.org/10.1039/b507137b>, 2005.

479 Castañeda, R., Iuga, C., Álvarez-Idaboy, J. R., and Vivier-Bunge, A.: Rate Constants and Branching Ratios in
480 the Oxidation of Aliphatic Aldehydes by OH Radicals under Atmospheric Conditions, J. Mex. Chem.
481 Soc., 56(3), 316–324, <https://doi.org/10.29356/jmcs.v56i3.296>, 2012.

482 Chacon-Madrid, H. J., Presto, A. A., and Donahue, N. M.: Functionalization vs. fragmentation: n-aldehyde
483 oxidation mechanisms and secondary organic aerosol formation, Phys. Chem. Chem. Phys., 12(42),
484 13975, <https://doi.org/10.1039/c0cp00200c>, 2010.

485 Ciccioli, P., Brancaleoni, E., Frattoni, M., Cecinato, A., and Brachetti, A.: Ubiquitous occurrence of semi-
486 volatile carbonyl compounds in tropospheric samples and their possible sources, Atmos. Environ. Part
487 A Gen. Top., 27(12), 1891–1901, [https://doi.org/10.1016/0960-1686\(93\)90294-9](https://doi.org/10.1016/0960-1686(93)90294-9), 1993.

488 Crounse, J. D., Knap, H. C., Ørnsø, K. B., Jørgensen, S., Paulot, F., Kjaergaard, H. G., and Wennberg, P. O.:
489 Atmospheric Fate of Methacrolein. 1. Peroxy Radical Isomerization Following Addition of OH and O₂,
490 J. Phys. Chem. A, 116(24), 5756–5762, <https://doi.org/10.1021/jp211560u>, 2012.

491 Crounse, J. D., Nielsen, L. B., Jørgensen, S., Kjaergaard, H. G., and Wennberg, P. O.: Autoxidation of Organic
492 Compounds in the Atmosphere, J. Phys. Chem. Lett., 4(20), 3513–3520,
493 <https://doi.org/10.1021/jz4019207>, 2013.

494 Da Silva, G.: Kinetics and Mechanism of the Glyoxal + HO₂ Reaction: Conversion of HO₂ to OH by Carbonyls,
495 J. Phys. Chem. A, 115(3), 291–297, <https://doi.org/10.1021/jp108358y>, 2011.

496 Duan, J., Tan, J., Yang, L., Wu, S., and Hao, J.: Concentration, sources and ozone formation potential of volatile
497 organic compounds (VOCs) during ozone episode in Beijing, *Atmos. Res.*, 88(1), 25–35,
498 <https://doi.org/10.1016/j.atmosres.2007.09.004>, 2008.

499 Ehn, M., Thornton, J. A., Kleist, E., Sipilä, M., Junninen, H., Pullinen, I., Springer, M., Rubach, F., Tillmann,
500 R., Lee, B., Lopez-Hilfiker, F., Andres, S., Acir, I.-H., Rissanen, M., Jokinen, T., Schobesberger, S.,
501 Kangasluoma, J., Kontkanen, J., Nieminen, T., Kurtén, T., Nielsen, L. B., Jørgensen, S., Kjaergaard, H.,
502 G., Canagaratna, M., Maso, M. D., Berndt, T., Petäjä, T., Wahner, A., Kerminen, V.-M., Kulmala, M.,
503 Worsnop, D. R., Wildt, J., and Mentel, T. F.: A large source of low-volatility secondary organic
504 aerosol, *Nature*, 506(7489), 476–479, <https://doi.org/10.1038/nature13032>, 2014.

505 Ervens, B., Sorooshian, A., Lim, Y. B., and Turpin, B. J.: Key parameters controlling OH-initiated formation of
506 secondary organic aerosol in the aqueous phase (aqSOA), *J. Geophys. Res. Atmos.*, 119(7), 3997–
507 4016, <https://doi.org/10.1002/2013JD021021>, 2014.

508 Ervens, B., Turpin, B. J., and Weber, R. J.: Secondary organic aerosol formation in cloud droplets and aqueous
509 particles (aqSOA): A review of laboratory, field and model studies, *Atmos. Chem. Phys.*, 11(21),
510 11069–11102, <https://doi.org/10.5194/acp-11-11069-2011>, 2011.

511 Fan, C., Yan, H., Wang, W., Sun, Z., and Ge, M.: Study on the reactions of n-pentanal and n-hexanal with Br
512 atoms: Kinetics, gas-phase products, and SOA formation, *Atmos. Environ.*, 339, 120869,
513 <https://doi.org/10.1016/j.atmosenv.2024.120869>, 2024.

514 Fry, J. L., Draper, D. C., Barsanti, K. C., Smith, J. N., Ortega, J., Winkler, P. M., Lawler, M. J., Brown, S. S.,
515 Edwards, P. M., Cohen, R. C., and Lee, L.: Secondary Organic Aerosol Formation and Organic Nitrate
516 Yield from NO₃ Oxidation of Biogenic Hydrocarbons, *Environ. Sci. Technol.*, 48(20), 11944–11953,
517 <https://doi.org/10.1021/es502204x>, 2014.

518 Gu, Y., Huang, R.-J., Duan, J., Xu, W., Lin, C., Zhong, H., Wang, Y., Ni, H., Liu, Q., Xu, R., Wang, L., and Li,
519 Y. J.: Multiple pathways for the formation of secondary organic aerosol in the North China Plain in
520 summer, *Atmos. Chem. Phys.*, 23(9), 5419–5433, <https://doi.org/10.5194/acp-23-5419-2023>, 2023.

521 Hallquist, M., Wenger, J. C., Baltensperger, U., Rudich, Y., Simpson, D., Claeys, M., Dommen, J., Donahue, N.
522 M., George, C., Goldstein, A. H., Hamilton, J. F., Herrmann, H., Hoffmann, T., Iinuma, Y., Jang, M.,
523 Jenkin, M. E., Jimenez, J. L., Kiendler-Scharr, A., Maenhaut, W., McFiggans, G., Mentel, Th. F.,
524 Monod, A., Prévôt, A. S. H., Seinfeld, J. H., Surratt, J. D., Szmigielski, R., and Wildt, J.: The

525 formation, properties and impact of secondary organic aerosol: Current and emerging issues, *Atmos.*
526 *Chem. Phys.*, 9(14), 5155–5236, <https://doi.org/10.5194/acp-9-5155-2009>, 2009.

527 Hansen, J. E., and Sato, M.: Trends of measured climate forcing agents, *P. Natl. Acad. of Sci.*, 98(26), 14778–
528 14783, <https://doi.org/10.1073/pnas.261553698>, 2001.

529 Hinsberg, W., and Houle, F.: Kinetiscope: A stochastic kinetics simulator, <http://hinsberg.net/kinetiscope> (last
530 access: 06 Nov 2023), 2022.

531 Huang, R.-J., Zhang, Y., Bozzetti, C., Ho, K.-F., Cao, J.-J., Han, Y., Daellenbach, K. R., Slowik, J. G., Platt, S.
532 M., Canonaco, F., Zotter, P., Wolf, R., Pieber, S. M., Bruns, E. A., Crippa, M., Ciarelli, G.,
533 Piazzalunga, A., Schwikowski, M., Abbaszade, G., Schnelle-Kreis, J., Zimmermann, R., An, Z., Szidat,
534 S., Baltensperger, U., El Haddad, I., and Prévôt, A. S. H.: High secondary aerosol contribution to
535 particulate pollution during haze events in China, *Nature*, 514(7521), 218–222,
536 <https://doi.org/10.1038/nature13774>, 2014.

537 Huang, W., Saathoff, H., Shen, X., Ramisetty, R., Leisner, T., and Mohr, C.: Chemical Characterization of
538 Highly Functionalized Organonitrates Contributing to Night-Time Organic Aerosol Mass Loadings and
539 Particle Growth, *Environ. Sci. Technol.*, 53(3), 1165–1174, <https://doi.org/10.1021/acs.est.8b05826>,
540 2019.

541 Iuga, C., Ignacio Sainz-Díaz, C., and Vivier-Bunge, A.: On the OH initiated oxidation of C2–C5 aliphatic
542 aldehydes in the presence of mineral aerosols, *Geochim. Cosmochim. Ac.*, 74(12), 3587–3597,
543 <https://doi.org/10.1016/j.gca.2010.01.034>, 2010.

544 Jacobson, M. C., Hansson, H. -C., Noone, K. J., and Charlson, R. J.: Organic atmospheric aerosols: Review and
545 state of the science, *Rev. Geophys.*, 38(2), 267–294, <https://doi.org/10.1029/1998RG000045>, 2000.

546 Jenkin, M. E., Derwent, R. G., and Wallington, T. J.: Photochemical ozone creation potentials for volatile
547 organic compounds: Rationalization and estimation, *Atmos. Environ.*, 163, 128–137,
548 <https://doi.org/10.1016/j.atmosenv.2017.05.024>, 2017.

549 Jokinen, T., Sipilä, M., Richters, S., Kerminen, V., Paasonen, P., Stratmann, F., Worsnop, D., Kulmala, M.,
550 Ehn, M., Herrmann, H., and Berndt, T.: Rapid Autoxidation Forms Highly Oxidized RO₂ Radicals in
551 the Atmosphere, *Angew. Chem. Int. Edit.*, 53(52), 14596–14600,
552 <https://doi.org/10.1002/anie.201408566>, 2014.

553 Kanakidou, M., Seinfeld, J. H., Pandis, S. N., Barnes, I., Dentener, F. J., Facchini, M. C., Van Dingenen, R.,
554 Ervens, B., Nenes, A., Nielsen, C. J., Swietlicki, E., Putaud, J. P., Balkanski, Y., Fuzzi, S., Horth, J.,

555 Moortgat, G. K., Winterhalter, R., Myhre, C. E. L., Tsigaridis, K., Vignati, E., Stephanou, E. G., and
556 Wilson, J.: Organic aerosol and global climate modelling: A review, *Atmos. Chem. Phys.*, 5(4), 1053–
557 1123, <https://doi.org/10.5194/acp-5-1053-2005>, 2005.

558 Kang, S., Wildt, J., Pullinen, I., Vereecken, L., Wu, C., Wahner, A., Zorn, S. R., and Mentel, T. F.: Formation of
559 highly oxygenated organic molecules from α -pinene photooxidation: Evidence for the importance of
560 highly oxygenated alkoxy radicals, *Atmos. Chem. Phys.*, 25(22), 15715–15740,
561 <https://doi.org/10.5194/acp-25-15715-2025>, 2025.

562 Kirkby, J., Duplissy, J., Sengupta, K., Frege, C., Gordon, H., Williamson, C., Heinritzi, M., Simon, M., Yan, C.,
563 Almeida, J., Tröstl, J., Nieminen, T., Ortega, I. K., Wagner, R., Adamov, A., Amorim, A.,
564 Bernhammer, A.-K., Bianchi, F., Breitenlechner, M., Brilke, S., Chen, X., Craven, J., Dias, A., Ehrhart,
565 S., Flagan, R. C., Franchin, A., Fuchs, C., Guida, R., Hakala, J., Hoyle, C. R., Jokinen, T., Junninen,
566 H., Kangasluoma, J., Kim, J., Krapf, M., Kürten, A., Laaksonen, A., Lehtipalo, K., Makhmutov, V.,
567 Mathot, S., Molteni, U., Onnela, A., Peräkylä, O., Piel, F., Petäjä, T., Praplan, A. P., Pringle, K., Rap,
568 A., Richards, N. A. D., Riipinen, I., Rissanen, M. P., Rondo, L., Sarnela, N., Schobesberger, S., Scott,
569 C. E., Seinfeld, J. H., Sipilä, M., Steiner, G., Stozhkov, Y., Stratmann, F., Tomé, A., Virtanen, A.,
570 Vogel, A. L., Wagner, A. C., Wagner, P. E., Weingartner, E., Wimmer, D., Winkler, P. M., Ye, P.,
571 Zhang, X., Hansel, A., Dommen, J., Donahue, N. M., Worsnop, D. R., Baltensperger, U., Kulmala, M.,
572 Carslaw, K. S., and Curtius, J.: Ion-induced nucleation of pure biogenic particles, *Nature*, 533(7604),
573 521–526, <https://doi.org/10.1038/nature17953>, 2016.

574 Kroll, J. H., and Seinfeld, J. H.: Chemistry of secondary organic aerosol: Formation and evolution of low-
575 volatility organics in the atmosphere, *Atmos. Environ.*, 42(16), 3593–3624,
576 <https://doi.org/10.1016/j.atmosenv.2008.01.003>, 2008.

577 Kuang, Y., He, Y., Xu, W., Yuan, B., Zhang, G., Ma, Z., Wu, C., Wang, C., Wang, S., Zhang, S., Tao, J., Ma,
578 N., Su, H., Cheng, Y., Shao, M., and Sun, Y.: Photochemical Aqueous-Phase Reactions Induce Rapid
579 Daytime Formation of Oxygenated Organic Aerosol on the North China Plain, *Environ. Sci. Technol.*,
580 54(7), 3849–3860, <https://doi.org/10.1021/acs.est.9b06836>, 2020.

581 Lee, B. H., Mohr, C., Lopez-Hilfiker, F. D., Lutz, A., Hallquist, M., Lee, L., Romer, P., Cohen, R. C., Iyer, S.,
582 Kurtén, T., Hu, W., Day, D. A., Campuzano-Jost, P., Jimenez, J. L., Xu, L., Ng, N. L., Guo, H., Weber,
583 R. J., Wild, R. J., Brown, S. S., Koss, A., de Gouw, J., Olson, K., Goldstein, A. H., Seco, R., Kim, S.,
584 McAvery, K., Shepson, P. B., Baumann, K., Edgerton, E., Liu, J., Shilling, J. E., Miller, D. O., Brune,

585 W. H., D'Ambro, E. L., and Thornton, J. A.: Highly functionalized organic nitrates in the southeast
586 United States: Contribution to secondary organic aerosol and reactive nitrogen budgets, *P. Natl. Acad.*
587 *Sci.*, 113(6), 1516–1521, <https://doi.org/10.1073/pnas.1508108113>, 2016.

588 Li, J., Zhai, C., Yu, J., Liu, R., Li, Y., Zeng, L., and Xie, S.: Spatiotemporal variations of ambient volatile
589 organic compounds and their sources in Chongqing, a mountainous megacity in China, *Sci. Total*
590 *Environ.*, 627, 1442–1452, <https://doi.org/10.1016/j.scitotenv.2018.02.010>, 2018.

591 Lipari, Frank., Dasch, J. M., and Scruggs, W. F.: Aldehyde emissions from wood-burning fireplaces, *Environ.*
592 *Sci. Technol.*, 18(5), 326–330, <https://doi.org/10.1021/es00123a007>, 1984.

593 Ma, Z., Liu, C., Zhang, C., Liu, P., Ye, C., Xue, C., Zhao, D., Sun, J., Du, Y., Chai, F., and Mu, Y.: The levels,
594 sources and reactivity of volatile organic compounds in a typical urban area of Northeast China, *J.*
595 *Environ. Sci.*, 79, 121–134, <https://doi.org/10.1016/j.jes.2018.11.015>, 2019.

596 Manion, J. A., Huie, R. E., Levin, R. D., Burgess Jr, D. R., Orkin, V. L., Tsang, W., McGivern, W. S., Hudgens,
597 J. W., Knyazev, V. D., Atkinson, D. B., Chai, E., Tereza, A. M., Lin, C.-Y., Allison, T. C., Mallard, W.
598 G., Westley, F., Herron, J. T., Hampson, R. F., and Frizzell, D. H.: NIST Chemical Kinetics Database,
599 NIST Standard Reference Database 17, version 7.0 (web version), release 1.6.8, data version 2015.09,
600 National Institute of Standards and Technology, MD, <https://kinetics.nist.gov/>, 2015.

601 McFiggans, G., Mentel, T. F., Wildt, J., Pullinen, I., Kang, S., Kleist, E., Schmitt, S., Springer, M., Tillmann, R.,
602 Wu, C., Zhao, D., Hallquist, M., Faxon, C., Le Breton, M., Hallquist, Å. M., Simpson, D., Bergström,
603 R., Jenkin, M. E., Ehn, M., Thornton, J. A., Alfarra, M. R., Bannan, T. J., Percival, C. J., Priestley, M.,
604 Topping, D., and Kiendler-Scharr, A.: Secondary organic aerosol reduced by mixture of atmospheric
605 vapours, *Nature*, 565(7741), 587–593, <https://doi.org/10.1038/s41586-018-0871-y>, 2019.

606 Mellouki, A., Le Bras, G., and Sidebottom, H.: Kinetics and Mechanisms of the Oxidation of Oxygenated
607 Organic Compounds in the Gas Phase, *Chem. Rev.*, 103(12), 5077–5096,
608 <https://doi.org/10.1021/cr020526x>, 2003.

609 Mellouki, A., Wallington, T. J., and Chen, J.: Atmospheric Chemistry of Oxygenated Volatile Organic
610 Compounds: Impacts on Air Quality and Climate, *Chem. Rev.*, 115(10), 3984–4014,
611 <https://doi.org/10.1021/cr500549n>, 2015.

612 Mentel, T. F., Springer, M., Ehn, M., Kleist, E., Pullinen, I., Kurtén, T., Rissanen, M., Wahner, A., and Wildt,
613 J.: Formation of highly oxidized multifunctional compounds: Autoxidation of peroxy radicals formed

614 in the ozonolysis of alkenes – deduced from structure–product relationships, *Atmos. Chem. Phys.*,
615 15(12), 6745–6765, <https://doi.org/10.5194/acp-15-6745-2015>, 2015.

616 Møller, K. H., Otkjær, R. V., Hyttinen, N., Kurtén, T., and Kjaergaard, H. G.: Cost-Effective Implementation of
617 Multiconformer Transition State Theory for Peroxy Radical Hydrogen Shift Reactions, *J. Phys. Chem.*
618 *A*, 120(51), 10072–10087, <https://doi.org/10.1021/acs.jpca.6b09370>, 2016.

619 Møller, K. H., Praske, E., Xu, L., Crouse, J. D., Wennberg, P. O., and Kjaergaard, H. G.: Stereoselectivity in
620 Atmospheric Autoxidation, *J. Phys. Chem. Lett.*, 10(20), 6260–6266,
621 <https://doi.org/10.1021/acs.jpcclett.9b01972>, 2019.

622 Nie, W., Yan, C., Yang, L., Roldin, P., Liu, Y., Vogel, A. L., Molteni, U., Stolzenburg, D., Finkenzeller, H.,
623 Amorim, A., Bianchi, F., Curtius, J., Dada, L., Draper, D. C., Duplissy, J., Hansel, A., He, X.-C.,
624 Hofbauer, V., Jokinen, T., Kim, C., Lehtipalo, K., Nichman, L., Mauldin, R. L., Makhmutov, V.,
625 Mentler, B., Mizelli-Ojdanic, A., Petäjä, T., Quéléver, L. L. J., Schallhart, S., Simon, M., Tauber, C.,
626 Tomé, A., Volkamer, R., Wagner, A. C., Wagner, R., Wang, M., Ye, P., Li, H., Huang, W., Qi, X.,
627 Lou, S., Liu, T., Chi, X., Dommen, J., Baltensperger, U., El Haddad, I., Kirkby, J., Worsnop, D.,
628 Kulmala, M., Donahue, N. M., Ehn, M., and Ding, A.: NO at low concentration can enhance the
629 formation of highly oxygenated biogenic molecules in the atmosphere, *Nat. Commun.*, 14(1), 3347,
630 <https://doi.org/10.1038/s41467-023-39066-4>, 2023.

631 Öström, E., Putian, Z., Schurgers, G., Mishurov, M., Kivekäs, N., Lihavainen, H., Ehn, M., Rissanen, M. P.,
632 Kurtén, T., Boy, M., Swietlicki, E., and Roldin, P.: Modeling the role of highly oxidized
633 multifunctional organic molecules for the growth of new particles over the boreal forest region, *Atmos.*
634 *Chem. Phys.*, 17(14), 8887–8901, <https://doi.org/10.5194/acp-17-8887-2017>, 2017.

635 Praske, E., Otkjær, R. V., Crouse, J. D., Hethcox, J. C., Stoltz, B. M., Kjaergaard, H. G., and Wennberg, P. O.:
636 Atmospheric autoxidation is increasingly important in urban and suburban North America, *P. Natl.*
637 *Acad. Sci.*, 115(1), 64–69, <https://doi.org/10.1073/pnas.1715540115>, 2018.

638 Pullinen, I., Schmitt, S., Kang, S., Sarrafzadeh, M., Schlag, P., Andres, S., Kleist, E., Mentel, T. F., Rohrer, F.,
639 Springer, M., Tillmann, R., Wildt, J., Wu, C., Zhao, D., Wahner, A., and Kiendler-Scharr, A.: Impact
640 of NO_x on secondary organic aerosol (SOA) formation from α -pinene and β -pinene photooxidation:
641 The role of highly oxygenated organic nitrates, *Atmos. Chem. Phys.*, 20(17), 10125–10147,
642 <https://doi.org/10.5194/acp-20-10125-2020>, 2020.

643 Rissanen, M. P.: NO₂ Suppression of Autoxidation–Inhibition of Gas-Phase Highly Oxidized Dimer Product
644 Formation, *ACS Earth Space Chem.*, 2(11), 1211–1219,
645 <https://doi.org/10.1021/acsearthspacechem.8b00123>, 2018.

646 Rissanen, M. P., Kurtén, T., Sipilä, M., Thornton, J. A., Kangasluoma, J., Sarnela, N., Junninen, H., Jørgensen,
647 S., Schallhart, S., Kajos, M. K., Taipale, R., Springer, M., Mentel, T. F., Ruuskanen, T., Petäjä, T.,
648 Worsnop, D. R., Kjaergaard, H. G., and Ehn, M.: The Formation of Highly Oxidized Multifunctional
649 Products in the Ozonolysis of Cyclohexene, *J. Am. Chem. Soc.*, 136(44), 15596–15606,
650 <https://doi.org/10.1021/ja507146s>, 2014.

651 Rissanen, M. P., Kurtén, T., Sipilä, M., Thornton, J. A., Kausiala, O., Garmash, O., Kjaergaard, H. G., Petäjä,
652 T., Worsnop, D. R., Ehn, M., and Kulmala, M.: Effects of Chemical Complexity on the Autoxidation
653 Mechanisms of Endocyclic Alkene Ozonolysis Products: From Methylcyclohexenes toward
654 Understanding α -Pinene, *J. Phys. Chem. A*, 119(19), 4633–4650, <https://doi.org/10.1021/jp510966g>,
655 2015.

656 Schauer, J. J., Kleeman, M. J., Cass, G. R., and Simoneit, B. R. T.: Measurement of Emissions from Air
657 Pollution Sources. 1. C₁ through C₂₉ Organic Compounds from Meat Charbroiling, *Environ. Sci.*
658 *Technol.*, 33(10), 1566–1577, <https://doi.org/10.1021/es980076j>, 1999a.

659 Schauer, J. J., Kleeman, M. J., Cass, G. R., and Simoneit, B. R. T.: Measurement of Emissions from Air
660 Pollution Sources. 2. C₁ through C₃₀ Organic Compounds from Medium Duty Diesel Trucks, *Environ.*
661 *Sci. Technol.*, 33(10), 1578–1587, <https://doi.org/10.1021/es980081n>, 1999b.

662 Schauer, J. J., Kleeman, M. J., Cass, G. R., and Simoneit, B. R. T.: Measurement of Emissions from Air
663 Pollution Sources. 3. C₁–C₂₉ Organic Compounds from Fireplace Combustion of Wood, *Environ. Sci.*
664 *Technol.*, 35(9), 1716–1728, <https://doi.org/10.1021/es001331e>, 2001.

665 Seal, P., Barua, S., Iyer, S., Kumar, A., and Rissanen, M.: A systematic study on the kinetics of H-shift reactions
666 in pristine acyl peroxy radicals, *Phys. Chem. Chem. Phys.*, 25(41), 28205–28212,
667 <https://doi.org/10.1039/D3CP01833D>, 2023.

668 Seinfeld, J. H., and Pandis, S. N.: *Atmospheric chemistry and physics: From air pollution to climate change*, 3rd
669 edn., John Wiley & Sons, ISBN 9781118947401, 2016.

670 Shallcross, D., Teresarventosduran, M., Bardwell, M., Bacak, A., Solman, Z., and Percival, C.: A semi-
671 empirical correlation for the rate coefficients for cross- and self-reactions of peroxy radicals in the gas-
672 phase, *Atmos. Environ.*, 39(4), 763–771, <https://doi.org/10.1016/j.atmosenv.2004.09.072>, 2005.

673 Shen, H., Vereecken, L., Kang, S., Pullinen, I., Fuchs, H., Zhao, D., and Mentel, T. F.: Unexpected significance
674 of a minor reaction pathway in daytime formation of biogenic highly oxygenated organic compounds,
675 *Sci. Adv.*, 8(42), eabp8702, <https://doi.org/10.1126/sciadv.abp8702>, 2022.

676 Spracklen, D. V., Jimenez, J. L., Carslaw, K. S., Worsnop, D. R., Evans, M. J., Mann, G. W., Zhang, Q.,
677 Canagaratna, M. R., Allan, J., Coe, H., McFiggans, G., Rap, A., and Forster, P.: Aerosol mass
678 spectrometer constraint on the global secondary organic aerosol budget, *Atmos. Chem. Phys.*, 11(23),
679 12109–12136, <https://doi.org/10.5194/acp-11-12109-2011>, 2011.

680 Tröstl, J., Chuang, W. K., Gordon, H., Heinritzi, M., Yan, C., Molteni, U., Ahlm, L., Frege, C., Bianchi, F.,
681 Wagner, R., Simon, M., Lehtipalo, K., Williamson, C., Craven, J. S., Duplissy, J., Adamov, A.,
682 Almeida, J., Bernhammer, A.-K., Breitenlechner, M., Brilke, S., Dias, A., Ehrhart, S., Flagan, R. C.,
683 Franchin, A., Fuchs, C., Guida, R., Gysel, M., Hansel, A., Hoyle, C. R., Jokinen, T., Junninen, H.,
684 Kangasluoma, J., Keskinen, H., Kim, J., Krapf, M., Kürten, A., Laaksonen, A., Lawler, M., Leiminger,
685 M., Mathot, S., Möhler, O., Nieminen, T., Onnela, A., Petäjä, T., Piel, F. M., Miettinen, P., Rissanen,
686 M. P., Rondo, L., Sarnela, N., Schobesberger, S., Sengupta, K., Sipilä, M., Smith, J. N., Steiner, G.,
687 Tomè, A., Virtanen, A., Wagner, A. C., Weingartner, E., Wimmer, D., Winkler, P. M., Ye, P., Carslaw,
688 K. S., Curtius, J., Dommen, J., Kirkby, J., Kulmala, M., Riipinen, I., Worsnop, D. R., Donahue, N. M.,
689 and Baltensperger, U.: The role of low-volatility organic compounds in initial particle growth in the
690 atmosphere, *Nature*, 533(7604), 527–531, <https://doi.org/10.1038/nature18271>, 2016.

691 Vereecken, L., and Peeters, J.: Decomposition of substituted alkoxy radicals—part I: A generalized structure–
692 activity relationship for reaction barrier heights, *Phys. Chem. Chem. Phys.*, 11(40), 9062,
693 <https://doi.org/10.1039/b909712k>, 2009.

694 Wang, S., Davidson, D. F., and Hanson, R. K.: High temperature measurements for the rate constants of C₁–C₄
695 aldehydes with OH in a shock tube, *Proc. Combust. Inst.*, 35(1), 473–480,
696 <https://doi.org/10.1016/j.proci.2014.06.112>, 2015.

697 Wang, Z., Ehn, M., Rissanen, M. P., Garmash, O., Quéléver, L., Xing, L., Monge-Palacios, M., Rantala, P.,
698 Donahue, N. M., Berndt, T., and Sarathy, S. M.: Efficient alkane oxidation under combustion engine
699 and atmospheric conditions, *Commun. Chem.*, 4(1), 18, <https://doi.org/10.1038/s42004-020-00445-3>,
700 2021.

701 Wildt, J., Mentel, T. F., Kiendler-Scharr, A., Hoffmann, T., Andres, S., Ehn, M., Kleist, E., Müsgen, P., Rohrer,
702 F., Rudich, Y., Springer, M., Tillmann, R., and Wahner, A.: Suppression of new particle formation

703 from monoterpene oxidation by NO_x, *Atmos. Chem. Phys.*, 14(6), 2789–2804,
704 <https://doi.org/10.5194/acp-14-2789-2014>, 2014.

705 Williams, I. D., Revitt, D. M., and Hamilton, R. S.: A comparison of carbonyl compound concentrations at
706 urban roadside and indoor sites, *Sci. Total Environ.*, 189–190, 475–483, [https://doi.org/10.1016/0048-](https://doi.org/10.1016/0048-9697(96)05248-5)
707 [9697\(96\)05248-5](https://doi.org/10.1016/0048-9697(96)05248-5), 1996.

708 Yan, C., Nie, W., Vogel, A. L., Dada, L., Lehtipalo, K., Stolzenburg, D., Wagner, R., Rissanen, M. P., Xiao, M.,
709 Ahonen, L., Fischer, L., Rose, C., Bianchi, F., Gordon, H., Simon, M., Heinritzi, M., Garmash, O.,
710 Roldin, P., Dias, A., Ye, P., Hofbauer, V., Amorim, A., Bauer, P. S., Bergen, A., Bernhammer, A.-K.,
711 Breitenlechner, M., Brilke, S., Buchholz, A., Mazon, S. B., Canagaratna, M. R., Chen, X., Ding, A.,
712 Dommen, J., Draper, D. C., Duplissy, J., Frege, C., Heyn, C., Guida, R., Hakala, J., Heikkinen, L.,
713 Hoyle, C. R., Jokinen, T., Kangasluoma, J., Kirkby, J., Kontkanen, J., Kürten, A., Lawler, M. J., Mai,
714 H., Mathot, S., Mauldin, R. L., Molteni, U., Nichman, L., Nieminen, T., Nowak, J., Ojdanic, A.,
715 Onnela, A., Pajunoja, A., Petäjä, T., Piel, F., Quéléver, L. L. J., Sarnela, N., Schallhart, S., Sengupta,
716 K., Sipilä, M., Tomé, A., Tröstl, J., Väisänen, O., Wagner, A. C., Ylisirniö, A., Zha, Q., Baltensperger,
717 U., Carslaw, K. S., Curtius, J., Flagan, R. C., Hansel, A., Riipinen, I., Smith, J. N., Virtanen, A.,
718 Winkler, P. M., Donahue, N. M., Kerminen, V.-M., Kulmala, M., Ehn, M., and Worsnop, D. R.: Size-
719 dependent influence of NO_x on the growth rates of organic aerosol particles, *Sci. Adv.*, 6(22),
720 [eaay4945](https://doi.org/10.1126/sciadv.aay4945), <https://doi.org/10.1126/sciadv.aay4945>, 2020.

721 Yang, X., Wang, H., Lu, K., Ma, X., Tan, Z., Long, B., Chen, X., Li, C., Zhai, T., Li, Y., Qu, K., Xia, Y.,
722 Zhang, Y., Li, X., Chen, S., Dong, H., Zeng, L., and Zhang, Y.: Reactive aldehyde chemistry explains
723 the missing source of hydroxyl radicals, *Nat. Commun.*, 15(1), 1648, [https://doi.org/10.1038/s41467-](https://doi.org/10.1038/s41467-024-45885-w)
724 [024-45885-w](https://doi.org/10.1038/s41467-024-45885-w), 2024.

725 Zhang, X., Cappa, C. D., Jathar, S. H., McVay, R. C., Ensberg, J. J., Kleeman, M. J., and Seinfeld, J. H.:
726 Influence of vapor wall loss in laboratory chambers on yields of secondary organic aerosol, *P. Natl.*
727 *Acad. Sci.*, 111(16), 5802–5807, <https://doi.org/10.1073/pnas.1404727111>, 2014.

728 Ziemann, P. J., and Atkinson, R.: Kinetics, products, and mechanisms of secondary organic aerosol formation,
729 *Chem. Soc. Rev.*, 41(19), 6582, <https://doi.org/10.1039/c2cs35122f>, 2012.

730